Appl. Phys. B 58, 289–294 (1994)

Applied Physics B Lasers and Optics

Spatial Distribution of YO Molecules Ejected from Laser-Ablated $YBa_2Cu_3O_{7-x}$

W. K. A. Kumuduni, Y. Nakata, T. Okada, M. Maeda

Department of Electrical Engineering, Kyushu University, Hakozaki, Fukuoka 812, Japan (Tel.: +81-92/641-1101, Fax: +81-92/631-2790)

Received 13 October 1993/Accepted 16 December 1993

Abstract. One-dimensional imaging laser-induced fluorescence spectroscopy has been used for in-situ measurements of spatial distributions of YO molecules produced during the ArF-laser ablation of $YBa_2Cu_3O_{7-x}$ in vacuum and oxygen gas environment. The time-integrated angular distribution of particles ejected in vacuum has a $\cos^n\theta$ form, where $11 < n < 13$. When oxygen gas was introduced, YO molecules were confined in a smaller volume, and temporal changes of their spatial distribution were interpreted in terms of blast-wave formation.

PACS: 52.00, 81.60

Pulsed-Laser Deposition (PLD) has been recognized as a potential method to deposit high-Temperature superconducting (high-T_c) thin films with high quality. One of the disadvantages in PLD is the inhomogeneity in the thickness distribution or in the composition of the deposited films, when one tries to deposit films over large areas. This problem may be solved by scanning of the substrate [1, 2] or by scanning of the ablation-laser beam [3]. In this case, the knowledge of the thickness distribution of the films deposited without scanning is of primary importance in the engineering design of the scanning system.

Thickness and composition distributions of high-T_c films have been investigated by analyzing the deposited films [4, 5] and theoretical considerations have been reported [6, 7]. To clarify the origin of the inhomogeneity of the deposited films, it is essential to understand the behavior of the particles ejected from an ablated target. A number of works have been reported on the behavior of particles in PLD using a variety of diagnostic techniques such as emission spectroscopy [8–10], mass spectroscopy [11] and laser spectroscopy [12–15]. However, most of them were concerned with the transport of the ablated particles along the target–substrate direction or the identification of the constituents in the ablated plume.

In this study, one-Dimensional Laser-Induced Fluorescence (1D-LIF) spectroscopy was applied to investigate the behavior of the ground state YO molecules ejected from a $YBa_2Cu_3O_{7-x}$ target. Spatial distributions along the target normal as well as in a plane parallel to the target surface were measured in a single laser shot and their temporal developments were also measured. In vacuum, the time-integrated angular distribution of YO molecules was well described by a $\cos^n\theta$ distribution with $n = 11$–13. When oxygen gas was introduced, the spatial distribution was constrained in a narrower volume and the temporal behavior was affected very much by oxygen pressure. The behavior in ambient oxygen gas was interpreted based on the formation of the blast wave.

1 Experimental Setup

The experimental arrangement is shown in Fig. 1. A sintered $YBa_2Cu_3O_{7-x}$ (YBCO) pellet (PSC-0130, Dowa Mining Co. Ltd.) on a rotating holder was ablated by focusing an ArF excimer-laser beam (Lambda Physik EMG-201MSC) at an angle of about 30 degrees to the pellet normal. The ablation fluence was evaluated by the burn pattern on a Polaroid film and the laser energy measured inside the chamber. Under the present experimental condition the spot size on the film was 1.3 mm × 3.8 mm and the fluence was calculated to be 0.8 J/cm^2. Oxygen gas was continuously flowing through the chamber, and its pressure was measured by a capacitance manometer. The pellet surface was polished with an 800 grits SiC emery paper before each experiment.

A XeCl excimer-laser-pumped dye-laser beam was passed 30 mm above and parallel to the target surface. Ground-state YO molecules were excited by tuning the wavelength of the dye laser on the $Q_1 + {}^QR_{12}$ (0, 0) band of the $A^2\Pi_{1/2} - X^2\Sigma$ transition of YO which was around 613.2 nm. The resultant fluorescence from a length of 20 mm along the probe dye-laser beam with the center at the target normal was imaged onto a photoelectric surface of a gated-image intensifier (Hamamatsu PM3323) through a slit of 1 mm in width. An intensified image was detected by an uncooled linear photodiode-array detector (Hamamatsu C2925), which was initialized before each laser shot to prevent the accumulation of dark current, and the

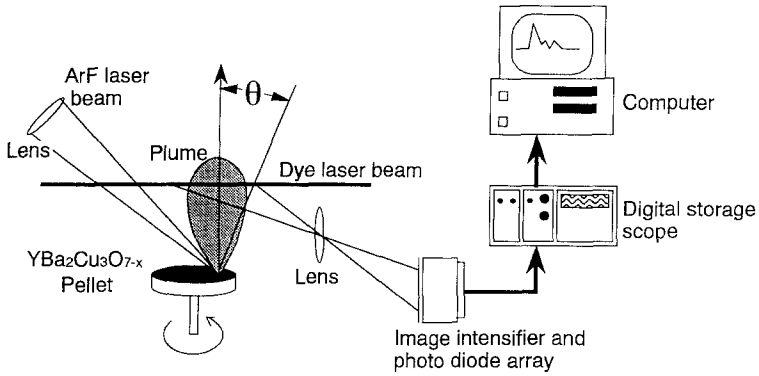

Fig. 1. Experimental arrangement. YO molecules along the probe dye-laser beam were measured using 1D-LIF

electrical signals were fed into a digital storage oscilloscope (Philips PM3320A). Signals were averaged over 4–16 shots in the digital storage oscilloscope and then stored in a personal computer (NEC PC9801). To reduce the background light from the plume, the gate duration of the intensifier was shortened to 60 ns, which is longer than the lifetime of the $A^2\Pi_{1/2}$ state of YO which is around 30 ns [16]. The spatial distribution of YO was measured in vacuum and in oxygen gas, varying the pressure from vacuum to 1 Torr. The temporal change of the spatial distribution has been recorded by varying the delay time between the ArF and the dye-laser shots using a preset delayed trigger pulser (SRS DG535). The ranges of parameters such as ablation fluence and oxygen pressures in the present experiment have been selected referring to [17].

2 Results and Discussion

2.1 Spatial Distribution of YO *in Vacuum*

Spatial distributions of YO molecules measured in vacuum at different delay times after the ablation are shown in Fig. 2. The YO molecules reached the observation area at about 3 μs after the ablation and signal intensity reached its maximum at around 7 μs, then decreased gradually. The most probable speed of the molecules was calculated to be 4.2×10^3 m/s, which is comparable with those reported for non-emissive neutral particles emitted in PLD [8, 18].

As can be seen in Fig. 2, the spatial distributions measured at 30 mm above the target surface vary with the arrival time. These distributions were used to evaluate the total number of particles which passed across the probe beam. Here the signal intensities were multiplied by the velocities of particles and integrated over the full observation time of 50 μs. The velocities of particles were calculated from the flight distance of 30 mm and the flight times. These calculations were performed for different horizontal positions along the probe beam. The values reflect the thickness distribution of the deposited films on the substrate, if the substrate is placed along the probe-laser beam and assuming the sticking coefficient of the particles is unity.

The integrated values are normalized and plotted in Fig. 3 by circles as a function of ejection angle θ, where θ is measured form the target normal, as shown in Fig. 1. When the ejection of particles is isotropic as in the thermal evaporation, the distribution should follow the $\cos^4\theta$ form

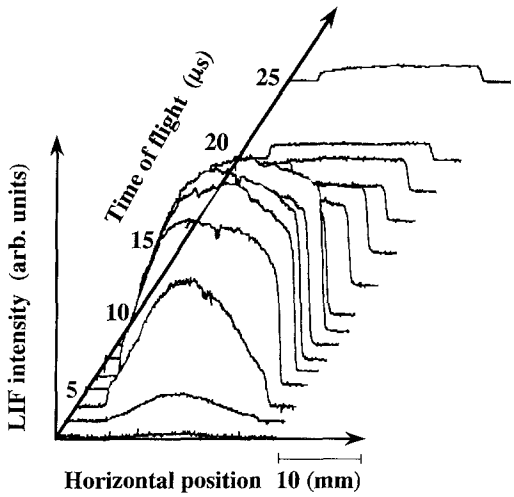

Fig. 2. Temporal change of spatial distribution of YO measured 30 mm above and parallel to the target surface in vacuum

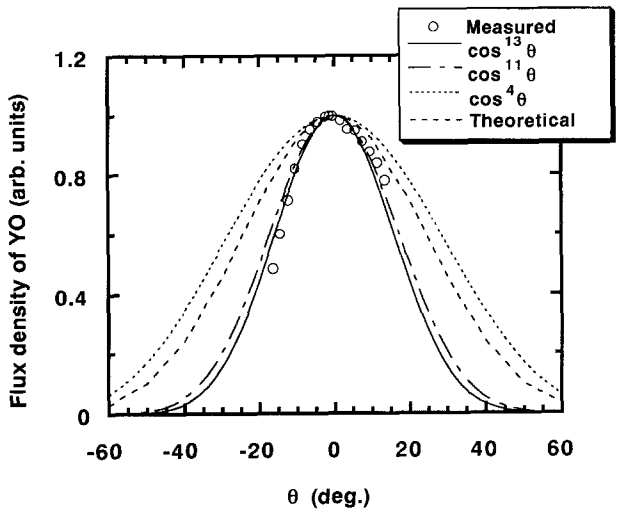

Fig. 3. Fit of the calculated deposit profile using (2) to the measured angular distribution. Also $\cos^4\theta$, $\cos^{11}\theta$ and $\cos^{13}\theta$ distributions are shown as references

which is shown by the dotted line in Fig. 3, as a reference. The departure of the measured values from the $\cos^4\theta$ is apparent, and the ejection of the YO molecules is highly forward-peaked normal to the target surface. This forward peaking is typical in pulsed-laser ablation. It is reported

that a part of the thickness distribution of the deposited film can be described by the higher orders of cos θ distribution in PLD [4, 5]. The present measurement best fitted with $n = 13$, as shown by the solid line in Fig. 3, based on the least-squares method. $n = 11$ gave a better fit for the distribution within an angle of less than 10°. The present values of $n = 11$–13 for the ground-state YO molecules are consistent with those reported previously for $8 < n < 14$ [4, 5], which have been obtained by measuring the thickness distribution of the YBCO films produced in excimer-laser ablation.

A model for the thickness distribution of pulsed-laser deposited films has been reported by Saenger [7], based on a velocity distribution function of laser-ablated particles. Starting with the shifted Maxwellian velocity distribution given by

$$f(v_x, v_y, v_z)dv_x dv_y dv_z = Be^{-[(m/2kT)(v_x^2+v_y^2+(v_z-u)^2]}dv_x dv_y dv_z , \quad (1)$$

the deposit thickness distribution $D(\theta)$ has been obtained as the following function assuming that the particles are ablated from a point source and have unit sticking coefficient on the substrate

$$D(\theta) = \frac{B'}{h^2}\cos^4\theta e^{-X^2\sin^2\theta}\int_0^\infty s^3 e^{-(s-X\cos\theta)^2}ds , \quad (2)$$

where v_x, v_y and v_z are the particle velocity components in Cartesian coordinates, T stands for the temperature corresponding to the velocity spread, u is the flow velocity, m is the particle mass, k is the Boltzmann constant, $s = v/(2kT/m)^{1/2}$, where v is the particle speed, $X = u/(2kT/m)^{1/2}$, h is the distance between the substrate and the target surface, and B and B' are normalization constants. The deposit thickness distribution is mainly controlled by the value of X, which is the ratio of the flow velocity to the random thermal velocity. That is, the thickness distribution is determined by how fast the particles flow onto the substrate before spreading out due to the isotropic thermal motion. When the flow velocity is zero, as in the thermal effusion, the thickness distribution of (2) turns to a $\cos^4\theta$ distribution.

The angular distribution in Fig. 3 was analyzed based on (2). For this purpose, the flow velocity of u and the temperature T should be known. These values were determined by the Time-Of-Flight (TOF) analysis. The TOF distribution was obtained from the data shown in Fig. 2 by plotting the signal intensities at the center of the observation line as a function of the flight time. The TOF distribution thus obtained is shown in Fig. 4. They were least-squares fitted with the velocity distribution of (1) setting $v_x = v_y = 0$, because data were taken on the axis of target normal. Such a fitting curve is shown by the solid line in Fig. 4, where u and T were 1.0 km/s and 3.0×10^4 K, respectively. These values are comparable with those measured earlier for particles ablated from YBCO [13, 19].

Substituting the values of u and T obtained into (2), the thickness distribution was calculated as a function of θ and shown by the dashed line in Fig. 3. The proposed model reasonably described the distribution around target normal, but the departure was observed at ejection angles of larger than 10 degrees. The whole distribution is described

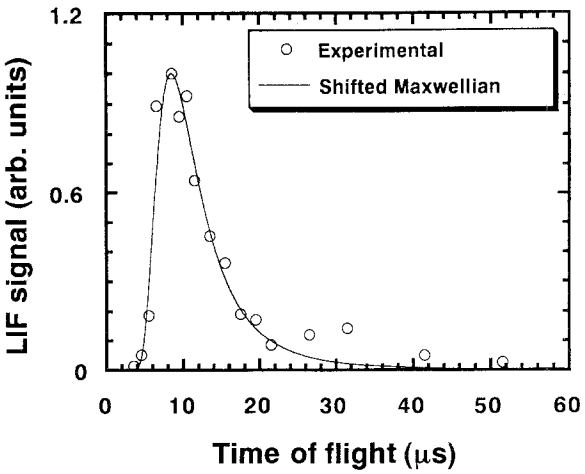

Fig. 4. TOF distribution of YO molecules in vacuum. The *solid line* is a shifted Maxwellian which corresponds to a temperature of 3.0×10^4 K and a flow velocity of 1.0 km/s

rather well with the simple $\cos^{13}\theta$ distribution, as described above. The following reason might be responsible for the discrepancy at large ejection angles. The TOF temperature T was calculated only for the particles on the deposition axes, and also the velocity components parallel to the target surface (v_x and v_y) were neglected. Thus, the calculated temperature may not be accurate enough especially for the off-axes molecules giving rise the above deviation at larger angles. Another possibility is that the temperature may have changed with time during the actual ablation, although a constant temperature is assumed in the present case.

2.2 *Distribution in Ambient Oxygen Gas*

In this section, the influence of the ambient gas on the YO density distribution is investigated. The distribution of particles in the presence of oxygen changed very much from that in vacuum. Spatial distributions of YO molecules measured in ambient oxygen gas at different delay times after the ablation are shown in Fig. 5a–d for oxygen gas pressures of 100 mTorr, 300 mTorr, 500 mTorr and 1 Torr, respectively.

At 100 mTorr, the onset of the signal was delayed and the signals were steeper, compared with those in vacuum. The horizontal span of the distributions were narrower than in vacuum. After a delay time of 8 μs, hollow distributions with peaks at the edges of the observation line were observed, as can be clearly seen in Fig. 5a. A similar tendency was observed at 300 mTorr oxygen gas pressure, as shown in Fig. 5b. The onset time delayed further, the horizontal span became narrower and a trace of the hollow distribution was still observed. At 500 mTorr, it can be seen that the signals built up slowly with further delayed signal onset. This tendency was enhanced when the oxygen pressure increased, as can be seen in 1 Torr distributions where the temporal change of the signals is very slow compared with those at lower pressures. The variation of distributions as the pressure is increased can be considered as the effect of the collisions between the ablated particles

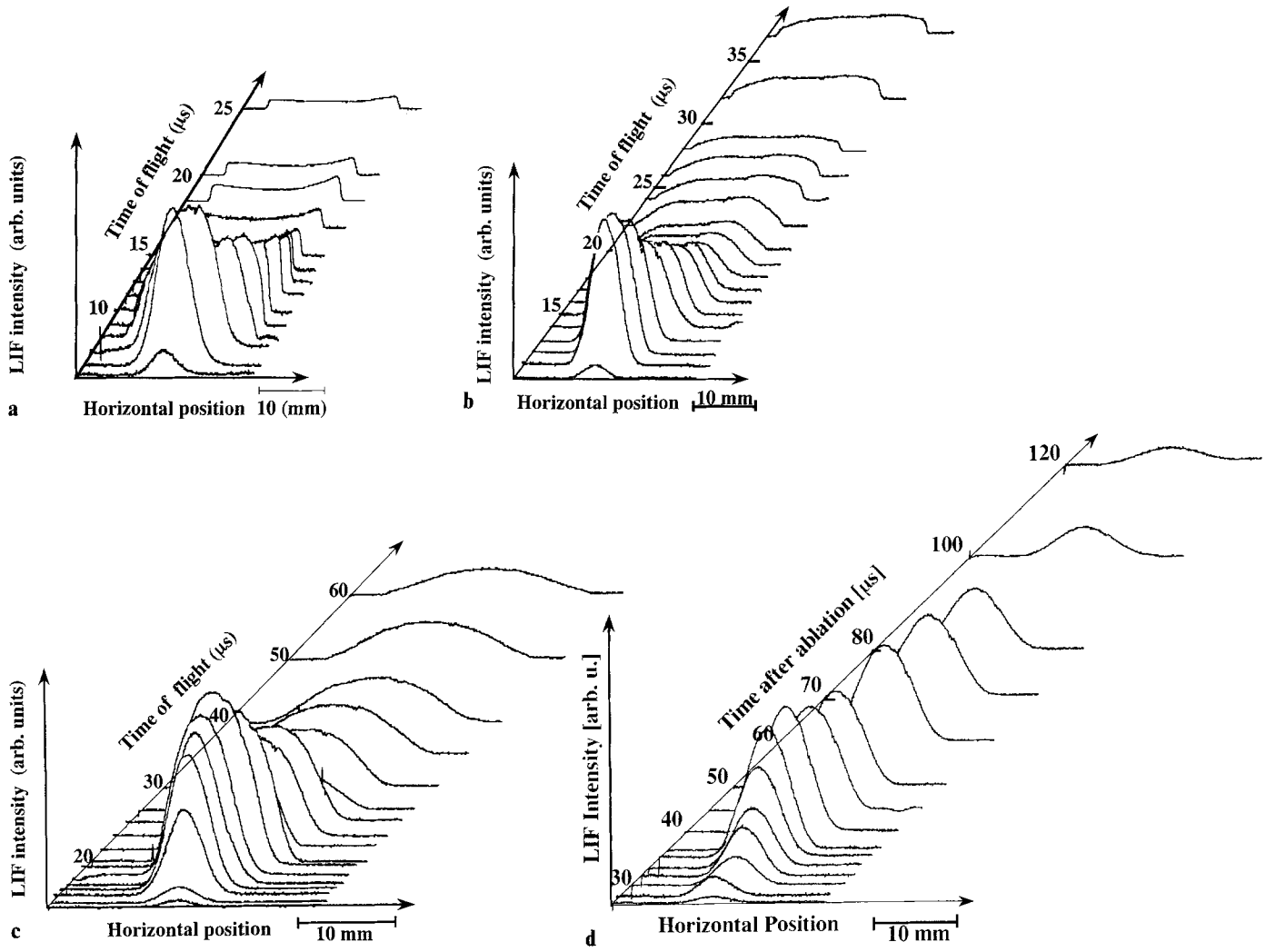

Fig. 5a–d. Temporal change of spatial distribution of YO molecules measured 30 mm above and parallel to the target surface at oxygen gas pressures of **a** 100 mTorr, **b** 300 mTorr, **c** 500 mTorr and **d** 1 Torr

and the background oxygen gas. This structure is briefly explained bellow.

It may be possible that the distributions become hollow due to spectroscopic effects such as reabsorption and quenching. In the present observations at 100 mTorr and 300 mTorr signal intensities at the edges of the distributions were compared for the equally spanned distributions and it was found that the intensity at 300 mTorr is higher than that at 100 mTorr by a factor of about 1.7. Therefore as far as reabsorption is concerned, absorption should be higher in the case of 300 mTorr which can not be seen in the 300 mTorr distributions, implying that the reabsorption has no effect on the hollowing of the distributions. The collisions between ablated particles and background gas at the periphery of the plume may cause quenching. If collisional quenching takes place, distribution turns to be hump rather than hollow. So other effects must be considered to investigate the hollow distributions.

It has been known for many decades that the blast waves can be driven in laser ablation in gas ambients. The initiation of blast waves during the actual PLD process of high-T_c superconducting thin films has not been fully recognized, but recent studies have revealed the presence of blast waves in PLD [18, 20]. It has been found in a series of experiments that the propagation of YO molecules over some limited flight distances from the target are well described by a point-source blast-wave model [21, 22]. Once the blast wave has fully developed in the PLD environment, the ejected particles push and compress the ambient oxygen gas in front of them just as a piston, and ejected particles concentrated near the boundary of the compressed oxygen layer, the so-called contact front. This structure is schematically shown in Fig. 6. The present 1D-LIF images at different delay times give the cross-sectional distributions at different positions of the plume, as the plume propagates, as shown in Fig. 6 by lines $L1$, $L2$ etc. corresponding to delay times t_1, t_2 etc. Which line of L_n can be observed at a given delay time depends on the speed of the particle plume.

For better understanding of the temporal changes observed in Fig. 5a–d, the propagation characteristics of the plume along the target normal has to be known. Such characteristics are shown in Fig. 7, where the 1D-LIF images of YO density distributions along the target normal were measured, exciting the YO molecules by a sheet dye-laser beam which was passed through the target normal. The laser energy was 0.4 J/cm^2. Spatial distributions

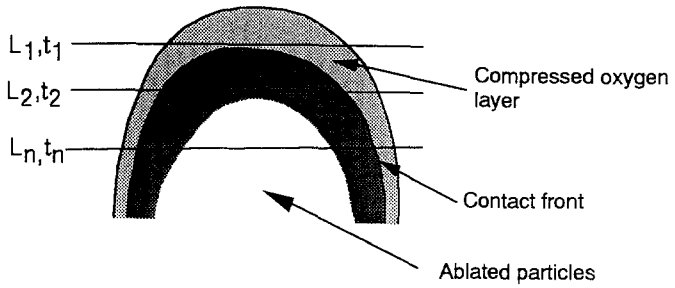

Fig. 6. Schematics of the expanding plume in oxygen gas ambients

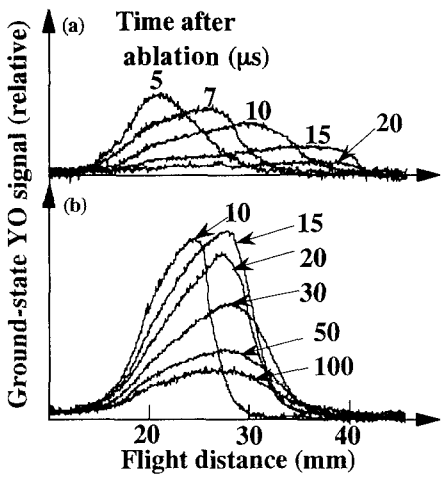

Fig. 7a, b. Temporal change of spatial distribution of particles measured along the target normal at oxygen gas pressures of 50 mTorr **a** and 300 mTorr **b**. Observation area was roughly from 15 mm to 42 mm along the target normal

at different delay times are summarized in Fig. 7, where the upper traces were obtained at an oxygen pressure of 50 mTorr and the lower at 300 mTorr. At 50 mTorr, particles completely flew across the observation area which was 15 mm to 42 mm along the target normal. At 300 mTorr, the speed of the particle plume was decelerated during the flight, and then the propagation of the particles finally stopped. Afterwards, the position of the peak of the distribution was stationary while the distributions became broadened with decrease in intensity, indicating that the diffusion was started. The maximum propagation distance became shorter as the oxygen pressure increased. The characteristics of the propagation measured along the target normal will be reported in detail elsewhere. [22]

The characteristics of distributions shown in Fig. 5a–d can be understood as follows. At an oxygen pressure of 100 mTorr and 300 mTorr, the plume propagated beyond the position of the dye-laser beam which is 30 mm from the target surface. It is thought that the steep built-up of the signals with time, observed at an oxygen pressure of 100 mTorr and 300 mTorr, is reflecting the structure of the contact front. And the hollow distributions observed at 100 mTorr indicates that the contact front is curved just as the contact front depicted in Fig. 6. This structure is consistent with the recent observation of fast photography of emissive particles [23], which shows the structure of the shock waves in front of the contact front. As the contact front passed beyond the observation position, the density of YO molecules rapidly decreased, as observed in the distributions at 100 mTorr and 300 mTorr at large delay times.

At 500 mTorr an 1 Torr, on the other hand, the peak position of the plume stopped just at the position of the dye laser beam, or the tip of the plume just reached the observation line. Afterwards the density distribution of YO is mainly controlled by diffusion and resulted in the slow temporal change. This has been clearly observed in the measurements of spatial distribution along the target normal [22] and examples of distributions measured at 50 mTorr and 300 mTorr are shown in Fig. 7. From the present observation, it is understood that the thickness profile of the deposited films is largely affected by where the substrate is placed relative to the finite propagation distance.

In conclusion, the spatial distribution of particles ejected in pulsed laser ablation of YBCO has been investigated by 1D-LIF spectroscopy. The time-integrated angular distribution of particles has a $\cos^{11-13}\theta$ distribution in vacuum. The spatial distribution of particles in oxygen backgrounds has also been reported, showing clearly that the particles propagate over a finite distance. Therefore, the deposition process and the resulting thickness distribution of the films will be greatly affected by the relative position between the propagation distance and the position of substrate. In order to evaluate the thickness profile of the deposited film in PLD environments, the effect of the diffusion should be considered, besides the distribution of particles in the ablated plume itself.

Acknowledgements. The authors would like to thank Y. Nakayama and Y. Sasaki for their help in the experiments and K. Muraoka for the loan of the ArF-excimer laser. This work was supported in part by a Grant-in-Aid from the Ministry of Education, Science and Culture of Japan.

References

1. S.R. Foltyn, R.E. Muenchausen, R.C. Dye, X.D. Wu, L. Luo, D.W. Cooke, R.C. Taber: Appl. Phys. Lett. **59**, 1374 (1991)
2. M.F. Davis, J. Wosik, K. Forster, S.C. Deshmukh, H.R. Rampersad, S. Shah, P. Siemsen, J.C. Wolfe, D.J. Economou: J. Appl. Phys. **69**, 7182 (1991)
3. J.A. Greer: J. Vac. Sci. Technol. A**10**, 1821 (1992)
4. T. Venkatesan, X.D. Wu, A. Inam, J.B. Wachtman: Appl. Phys. Lett. **52**, 1193 (1988)
5. X.D. Wu, S.R. Foltyn, R.C. Dye, A.R. Garcia, N.S. Nogar, R.E. Muenchausen: Thin Solid Films **218**, 310 (1992)
6. R.K. Singh, O.W. Holland, J. Narayan: J. Appl. Phys. **68**, 233 (1990)
7. K.L. Saenger: J. Appl. Phys. **70**, 5629 (1991)
8. C. Girault, D. Damiani, J. Aubreton, A. Catherinot: Appl. Phys. Lett. **55**, 182 (1989)
9. J.P. Zheng, Z.Q. Huang, D.T. Shaw, H.S. Kwok: Appl. Phys. Lett. **54**, 280 (1989)
10. W.A. Weimer: Appl. Phys. Lett. **52**, 2171 (1988)
11. C.H. Chen, T.M. Murphy, R.C. Phillips: Appl. Phys. Lett. **57**, 937 (1990)
12. C.E. Otis, R.W. Dreyfus: Phys. Rev. Lett. **67**, 2102 (1991)

13. T. Okada, N. Shibamaru, Y. Nakayama, M. Maeda: Appl. Phys. Lett. **60**, 941 (1992)
14. T. Okada, N. Shibamaru, Y. Nakayama, M. Maeda: Jpn. J. Appl. Phys. **31**, 367 (1992)
15. T. Okada, Y. Nakayama, Y. Nakata, W.K.A. Kumuduni, M. Maeda: Appl. Phys. Lett. **61**, 2368 (1992)
16. K. Liu, J.M. Parson: J. Chem. Phys. **67**, 1814 (1977)
17. T. Nagaishi, S. Itozaki: Rev. Laser Eng. **20**, 355 (1992) (in Japanese)
18. D.B. Geohegan: Appl. Phys. Lett. **60**, 2732 (1992)
19. C.E. Otis, P.M. Goodwin: J. Appl. Phys. **73**, 1957 (1993)
20. A. Gupta, B. Braren, K.G. Casey, B.W. Hussey, R. Kelly: Appl. Phys. Lett. **59**, 1302 (1991)
21. W.K.A. Kumuduni, Y. Nakayama, Y. Nakata, T. Okada, M. Maeda: Jpn. J. Appl. Phys. **32**, L271 (1993)
22. W.K.A. Kumuduni, Y. Nakata, T. Okada, M. Maeda: J. Appl. Phys. (1993) (in press)
23. D.B. Geohegan: Thin Solid Films **220**, 138 (1992)